

New observational constraints on interacting dark energy using galaxy clusters virial equilibrium states

M. Le Delliou,^{1,2,3}★ R. J. F. Marcondes⁴† and G. B. Lima Neto⁵

¹*Institute of Theoretical Physics, Physics Department, Lanzhou University, No.222, South Tianshui Road, Lanzhou, Gansu 730000, P R China*

²*Instituto de Astrofísica e Ciências do Espaço, Universidade de Lisboa, Faculdade de Ciências, Ed. C8, Campo Grande, 1769-016 Lisboa, Portugal*

³*Instituto de Física Teórica, Universidade Estadual de São Paulo (IFT-UNESP), Rua Dr. Bento Teobaldo Ferraz 271, Bloco 2 - Barra Funda, CEP 01140-070, São Paulo, SP, Brazil*

⁴*Instituto de Física, Universidade de São Paulo, Rua do Matão 1371, Cidade Universitária, CEP 05508-090, São Paulo, SP, Brazil*

⁵*Instituto de Astronomia, Geofísica e Ciências Atmosféricas, Universidade de São Paulo, Rua do Matão 1226, Cidade Universitária, CEP 05508-090, São Paulo, SP, Brazil*

Accepted XXX. Received YYY; in original form ZZZ

ABSTRACT

As the dark sector remains unknown in composition and interaction between dark energy and dark matter stand out as natural, observations of galaxy clusters out of equilibrium abound, opening a promising window on these questions. We continue here the exploration of dark sector interaction detection via clusters virial equilibrium state for all clusters configurations. The dynamics of clusters is evaluated with the Layzer-Irvine equation, a simple model of an interacting dark sector and some simplifying assumptions to obtain the time-dependent part of the virial dynamics. The clusters' data are concentrated in optical weak lensing and X-ray observations that evaluate, respectively, the clusters' mass profiles and temperatures. The global inconsistency of available X-ray data led us to constitute “gold” cluster samples. Through a Bayesian analysis, they are processed to obtain consistent interaction detected up to 3σ , in compounded interaction strength for 11 clusters at -0.027 ± 0.009 that translate in compounded universal equilibrium virial ratio of $-0.61_{-0.03}^{+0.04}$. The level of detection and inconsistency of X-ray data call for caution, although future instruments promise a clearer detection soon.

Key words: Gravitation – Galaxies: clusters: general – Cosmology: theory – dark energy – dark matter – large-scale structure of Universe.

1 INTRODUCTION

Since the discovery of cosmic acceleration (Perlmutter et al. 1999) and the proposal of dark energy (DE) as its source, in addition to the already sought dark matter (DM, Zwicky 1933, 1937), the largely unknown nature of the dark sector naturally called for possible interactions within its manifestations (Amendola 2000a,b).

Despite considerable efforts towards direct and indirect detection, the only evidence at hand of the existence of the dark sector remain purely gravitational, through the Cosmic Microwave Background observations (Ade et al. 2014), supernovae acceleration (Perlmutter et al. 1999; Riess et al. 1998) or clusters displaying segregated mass and baryons (dissociative clusters), such as the so-called “Bullet Cluster” (Clowe et al. 2006), “El Gordo” (Jee et al. 2014), Abell 1758 (Monteiro-Oliveira et al. 2017), among others. In this context, detection of interactions inside the dark sector would significantly help us understand the nature of dark matter and dark

energy and even increase the probability of these components to exist.

In a previous paper (Le Delliou et al. 2015, hereafter LeD15), we developed an approach to the detection of such interactions in the virial state of galaxy clusters, through a simplified coupled dark energy (CDE) cosmology model, coupled with the Layzer-Irvine dynamical virial equation. Based on a series of papers exploring such detection in apparently balanced clusters, and their check by other groups (Bertolami et al. 2007; Le Delliou et al. 2007; Bertolami et al. 2008, 2009, 2012; Abdalla et al. 2009, 2010; He et al. 2010), this latest approach attempted to include the effect of departure from equilibrium. However, although this allowed for the use in the detection of a wider sample of clusters, it involved the assumption that clusters present small departures from virial equilibrium, and found it to be the source of inconsistencies in the results. The present paper proposes now to remedy these inconsistencies by allowing larger departures in an evaluation independent from the astrophysical processes expected to source this deviation from balance. We also attempt a more robust statistical treatment of the data, with a Bayesian approach.

In the following section 2, the framework in which data will

★ E-mail: delliou@ift.unesp.br

† E-mail: rafaelmarcondes@usp.br

be analysed is laid out. The sample and statistical treatment are discussed in Sec. 3.1, while the analysis is described in Sec. 4. The results are discussed in Sec. 5 before to conclude in Sec. 6.

2 THE FRAMEWORK

2.1 The cosmological model

We model the universe, composed of dark matter and dark energy only, as a flat Friedmann-Lemaître-Robertson-Walker (FLRW) background metric. The dark sector interaction is modeled with a heat flux in the Bianchi identities between the two dark components, denoted by subscript c for cold DM and d for DE (i.e. energy conservation equations, linking the energy densities ρ evolutions, the DE equation of state $w_d = P_d/\rho_d$, P_d being the DE pressure, and the Hubble parameter H to the dark matter-dark energy interaction coupling ξ):

$$\dot{\rho}_c + 3H\rho_c = 3H\xi\rho_c, \quad \dot{\rho}_d + 3H\rho_d(1 + w_d) = -3H\xi\rho_c. \quad (1)$$

With this sign convention, positive ξ means that dark energy decays into dark matter. The equation-of-state parameter w_d is set to -1 in most of our analyses, except in one case where we make it a free parameter of the model. The rest of the FLRW evolution is standard.

2.2 The Layzer-Irvine equation

The Layzer-Irvine equation can be recast to relate the kinetic (ρ_K) and gravitational potential (ρ_W) parts of the dark matter density ρ_c of the studied, evolving system (a cluster). As a generalisation of the virial equation, it describes how the system tends to relax. In this CDE scenario, it has been obtained by He et al. (2010) as

$$\dot{\rho}_c + H[(2 + 3\xi)\rho_K + (1 - 6\xi)\rho_W] = 0. \quad (2)$$

In LeD15,¹ the condition of small departures from equilibrium was imposed, that led to the approximation $\dot{\rho}_K/\rho_K \approx \dot{\rho}_W/\rho_W$. In this work, the results from LeD15 require to allow the clusters to be away from equilibrium. Thus $\dot{\rho}_W$ and $\dot{\rho}_K$ will be modeled separately (see Sec. 2.2.2). Eq. (2) can be reformulated to give the out-of-equilibrium virial ratio

$$\frac{\rho_K}{\rho_W} = -\frac{1 - 6\xi}{2 + 3\xi} - \frac{1}{2 + 3\xi} \frac{\dot{\rho}_K + \dot{\rho}_W}{H\rho_W}. \quad (3)$$

This allows us to compare observed values of the virial ratio, built from the quantity ρ_K/ρ_W extracted from clusters and called hereafter the observed virial ratio (OVR), with a modified ratio involving the interaction coupling, which we will refer to as the equilibrium virial ratio (EVR),² and the time evolution term involving the time derivative, which we call departure from equilibrium (DfE). We propose to model and build the OVR and DfE from

¹ In LeD15, the choice of the coupling strengths $\xi_1 = \xi/18$ and $\xi_2 = -(\xi/6)\rho_c/\rho_d$ was inconsistent with the derivation of the Layzer-Irvine equation by He et al. (2010), which defines ξ_1 and ξ_2 to be constants. Here, we amend that mistake simply adopting $\xi_1 = \xi$ and $\xi_2 = 0$, which also makes the interaction dependent on the dark matter energy density only, but leads to a different Layzer-Irvine equation. Notice that the sign of the interacting term yields a positive flux $3H\xi\rho_c$ towards DM when all terms are positive, in agreement with common phenomenological descriptions of the interacting term in the literature (for instance He et al. 2010; Cao & Liang 2013; Costa et al. 2017).

² Formerly named theoretical virial ratio (TVR) in LeD15.

observations of clusters' mass M_{200} enclosed in a radius r_{200} ,³ the NFW concentration parameter c_{200} and the X-ray temperature T_X . The DfE will also depend on the parameter of interest ξ , on the density parameter Ω_{c0} and on $h \equiv H_0/100 \text{ km s}^{-1} \text{ Mpc}^{-1}$ that enter in the Hubble rate H . Rewriting Eq. (3) as

$$\frac{\rho_K}{\rho_W} + \frac{1}{2 + 3\xi} \frac{\dot{\rho}_K + \dot{\rho}_W}{H\rho_W} = -\frac{1 - 6\xi}{2 + 3\xi}, \quad (4)$$

explicit the universal, predicted equilibrium virial ratio (i.e., the kinetic to potential ratio that should be reached by a cluster at perfect equilibrium) that can be obtained from specific clusters' observed virial ratio minus departure from equilibrium in the left-hand side of Eq. (4). The first step is to evaluate the kinetic and potential energy densities. Then we need to evaluate in a sensible way the DfE term. Thus only remains to place constraints on the interaction coupling parameter ξ , which can be performed by Markov Chain Monte Carlo (MCMC) simulations.

2.2.1 The kinetic and potential energy densities

We follow LeD15 evaluations of these densities, from the measurements of the given cluster's X-ray temperature T_X , mass M_{200} and NFW concentration parameter c_{200} . The potential energy is approximated using the NFW density profile (Navarro et al. 1996) extracted from the cluster's observed mass and concentration (defining $c_{200} = r_{200}/r_0$ instead of using r_0). Thus, we have

$$\rho_W = -\frac{3GM_{200}^2}{4\pi r_{200}^4 f_c}, \quad (5)$$

with

$$f_c \equiv \frac{C^2/c_{200}}{\frac{1}{2}c_{200}^2 - C}, \quad C \equiv C' \ln C' - c_{200}, \quad C' \equiv 1 + c_{200}. \quad (6)$$

The kinetic energy is (LeD15)

$$\rho_K = \frac{9}{8\pi} \frac{M_{200} k_B T_X}{r_{200}^3 \mu m_H}, \quad (7)$$

where k_B is the Boltzmann constant, $\mu = 0.63$ is the intracluster plasma mean molecular weight (defined as the mean mass of the particles divided by the Hydrogen mass, assumed to be completely ionized and with primordial chemical composition), and m_H is the proton mass. The ratio of these two densities is the observed virial ratio

$$\frac{\rho_K}{\rho_W} = -\frac{3}{2} \frac{r_{200}}{GM_{200}} \frac{k_B T_X}{\mu m_H} f_c. \quad (8)$$

The radius r_{200} is evaluated from the NFW parameters (see footnote 3) with the critical density at the redshift of the cluster and in the same cosmology assumed by the observers to keep consistency with the fitted NFW profile.

2.2.2 Evaluating the departure from equilibrium

To allow for the extra freedom introduced by relaxing the small departures from equilibrium assumption, compared to LeD15, the virial ratio now depends on both temperature and virial radius, the concentration remaining a parameter. We note that both densities

³ Recall then that $M_{200}/\text{Vol}(r_{200}) = 200\rho_{cr}$ with the critical density $\rho_{cr} = 3H^2(z)/8\pi G$.

can be rewritten as functions of their local measured quantities, recognizing the critical density ratio definition in powers of mass and radius, as

$$\rho_K = \rho_K(T_X) = 300 \rho_{cr} \frac{k_B T_X}{\mu m_H} \quad (9)$$

and

$$\rho_W = \rho_W(r_{200}) = -(200 \rho_{cr})^2 G \frac{4\pi r_{200}^2}{3 f_c}. \quad (10)$$

We thus can compute the time derivatives of Eq. (3) as

$$\dot{\rho}_K + \dot{\rho}_W = \frac{d\rho_K}{dT_X} \dot{T}_X + \frac{d\rho_W}{dr_{200}} \dot{r}_{200}, \quad (11)$$

which is fully general, as opposed to the evaluation in LeD15. The delicate part is then to evaluate \dot{T}_X and \dot{r}_{200} . Based on the reasonable expectations from hierarchical structure formation that clusters' temperature and radius should evolve to equilibrium values, increasing faster in the past than in the future, we propose two physically reasonable ansätze which derivatives asymptote to zero from positive decreasing values, meaning that both T_X and r_{200} should increase to reach equilibrium, a behaviour which is observed in semi-analytical simulations (as can be seen from studying [Henriksen & Widrow 1995, 1997, 1999](#); [Del Popolo et al. 2000](#); [Le Delliou & Henriksen 2003](#); [MacMillan et al. 2006](#); [Le Delliou 2008](#)):

$$\dot{T}_X = \frac{T_X/t_0}{(t/t_0)^2}, \quad \dot{r}_{200} = \gamma \frac{r_{200}/t_0}{(t/t_0)^{\gamma+1}}, \quad (12)$$

derived respectively from heuristic exponential parametrizations $T_X = T_X^* \exp(-t_0/t)$ and $r_{200} = r_{200}^* \exp(-t_0/t)^\gamma$ ($\gamma \neq 1$), where T_X^* and r_{200}^* are the asymptotic equilibrium values and t_0 is some characteristic time scale. The parametrization is using the simplicity of the strong convergence of the exponential function (see, e.g. the fast virialization of haloes seen in [Henriksen & Widrow 1995](#), and their moderately violent relaxation) and the finite value convergence of the inverse power law. We further restrict our parametrization of γ to positive values so as to keep the approach of asymptotic growth of the radius towards r_{200}^* . When $\gamma < 1$ ($\gamma > 1$), the radius approaches the equilibrium faster (slower) than the temperature.⁴ These ansätze are used locally to give the evolution slopes but are not considered globally integrable. They provide one equation,

$$\frac{\dot{T}_X}{T_X/t_0} = \left(\frac{\dot{r}_{200}}{\gamma r_{200}/t_0} \right)^{\frac{2}{\gamma+1}}, \quad (13)$$

to obtain the unknown time evolutions \dot{T}_X and \dot{r}_{200} . The remaining equation needed to provide a solution in terms of observed values for these unknown can be chosen as the equation of state for the perfect gas, considered isobaric:

$$\frac{T_X}{r_{200}^3} = \text{constant}, \quad (14)$$

which can be derived into

$$\frac{\dot{T}_X}{\dot{r}_{200}} = 3 \frac{T_X}{r_{200}}. \quad (15)$$

Solving for the derivatives in terms of γ , T_X and r_{200} , the DFE term is given by

$$-\frac{\dot{\rho}_K + \dot{\rho}_W}{(2 + 3\xi) H \rho_W} = - \left(3 \frac{T_X}{\rho_W} \frac{d\rho_K}{dT_X} + \frac{r_{200}}{\rho_W} \frac{d\rho_W}{dr_{200}} \right) \frac{(\gamma^2 3^{\gamma+1})^{\frac{1}{1-\gamma}}}{(2 + 3\xi) H t_0}, \quad (16)$$

⁴ The two cases are better analysed separately due to divergences at $\gamma = 1$. For the sake of simplicity, in this work we consider only the first case.

with the derivatives given by

$$\frac{T_X}{\rho_W} \frac{d\rho_K}{dT_X} = \frac{\rho_K}{\rho_W} \frac{d \ln \rho_K}{d \ln T_X} = \frac{\rho_K}{\rho_W} \quad (17)$$

and

$$\frac{r_{200}}{\rho_W} \frac{d\rho_W}{dr_{200}} = 2 - \frac{d \ln f_c}{d \ln r_{200}} = 2 - \frac{d \ln f_c}{d \ln c_{200}}. \quad (18)$$

The exact time scale t_0 is not important to our purposes. Since this parameter only appears dividing $(\gamma^2 3^{\gamma+1})^{1/(1-\gamma)}$, it can be absorbed into this term with the only effect of shifting the value of γ at which its marginalized distribution becomes suppressed (as that term diverges with γ approaching the unity), so we set $t_0 = 1$ (in units of $\text{km}^{-1} \text{s Mpc}$).

3 THE DATA

We start from a sample of 50 clusters with weak-lensing mass measurements of M_{200} given by [Okabe & Smith \(2016\)](#) and corresponding measurements of c_{200} kindly provided by Okabe (private communication). The NFW profiles are based on a flat Λ CDM background cosmology with DM and DE density parameters $\Omega_{c0} = 0.3$ and $\Omega_{d0} = 0.7$, which we use in the evaluation of r_{200} . These data can be complemented with X-ray temperature data from a few different sources. By collecting temperature data from [Maughan et al. \(2012\)](#), [Martino et al. \(2014\)](#) or [Mantz et al. \(2016, 2017\)](#) (hereafter M12, M14 and M16, respectively), we end up with subsets of 22, 19 or 30 clusters. The data are summarized in table 1.

We note that uncertainties in M_{200} , c_{200} and $k_B T_X$ from M12 are generally asymmetrical, in the form $\bar{x}_{-\sigma_-}^{+\sigma_+}$. Since these quantities should be always positive and typically $\sigma_+ \geq \sigma_-$, it seems reasonable to assume that these 1σ -error measurements represent well 68.3 per cent credible intervals of lognormal distributions. As in LeD15, we want these lognormal distributions to have their parameters μ and σ adjusted to match the following conditions: (i) the maximum probability coincides with the nominal value \bar{x} , (ii) the probability of the random variable lying between $\bar{x} - \sigma_-$ and $\bar{x} + \sigma_+$ is 68.3 per cent and (iii) the probability density function has the same value at the points $\bar{x} - \sigma_-$ and $\bar{x} + \sigma_+$, so that the interval between them corresponds to the 68.3 per cent most likely values. For this, we write

$$\chi^2 = C_{(i)}^2 + C_{(ii)}^2 + C_{(iii)}^2, \quad (19)$$

where

$$C_{(i)} \equiv \frac{\exp(\mu - \sigma^2)}{\bar{x}} - 1, \quad (20)$$

$$C_{(ii)} \equiv \frac{f_{\mu,\sigma}(\bar{x} + \sigma_+)}{f_{\mu,\sigma}(\bar{x} - \sigma_-)} - 1, \quad (21)$$

$$C_{(iii)} \equiv \frac{F_{\mu,\sigma}(\bar{x} + \sigma_+) - F_{\mu,\sigma}(\bar{x} - \sigma_-)}{0.683} - 1 \quad (22)$$

represent the three conditions, with

$$f_{\mu,\sigma}(x) = \frac{1}{x\sigma\sqrt{2\pi}} \exp\left[-\frac{(\ln x - \mu)^2}{2\sigma^2}\right] \quad (23)$$

and

$$F_{\mu,\sigma}(x) = \frac{1}{2} \left[1 + \text{erf}\left(\frac{\ln x - \mu}{\sigma\sqrt{2}}\right) \right] \quad (24)$$

the lognormal probability (PDF) and cumulative (CDF) density functions, respectively. We then find, for each of these measurements, the pair of parameters (μ, σ) that minimizes χ^2 . The

Table 1. Redshift, NFW parameters from Okabe & Smith (2016) and temperature of galaxy clusters from different sources. Temperatures are given in keV and masses in units of $h^{-1}10^{14}M_{\odot}$.

Cluster	z	M_{200}	c_{200}	$k_{\text{B}}T_{\text{X}}$ (Maughan et al. 2012)	$k_{\text{B}}T_{\text{X}}$ (Martino et al. 2014)	$k_{\text{B}}T_{\text{X}}$ (Mantz et al. 2016, 2017)
ABELL0068	0.2546	$6.65^{+1.35}_{-1.16}$	$4.83^{+1.83}_{-1.31}$	7.8 ± 1.0	5.02 ± 1.65	9.62 ± 1.65
ABELL0115	0.1971	$7.04^{+2.66}_{-1.97}$	$1.59^{+1.12}_{-0.77}$	6.7 ± 0.3	6.46 ± 0.51	11.74 ± 0.90
ABELL0209	0.2060	$12.75^{+2.27}_{-1.91}$	$3.63^{+1.02}_{-0.84}$	7.4 ± 0.5	7.56 ± 1.40	8.98 ± 0.67
ABELL0267	0.2300	$5.96^{+1.16}_{-1.08}$	$3.16^{+1.01}_{-0.81}$	$4.4^{+0.5}_{-0.4}$	–	–
ABELL0383	0.1883	$5.23^{+1.30}_{-1.07}$	$4.12^{+2.06}_{-1.41}$	4.5 ± 0.3	5.76 ± 1.26	7.26 ± 0.42
ABELL0521	0.2475	$5.61^{+1.18}_{-1.05}$	$3.48^{+1.57}_{-1.09}$	4.8 ± 0.2	–	7.29 ± 0.25
ABELL0586	0.1710	$6.65^{+2.15}_{-1.61}$	$6.77^{+6.83}_{-3.36}$	7.6 ± 0.8	–	7.40 ± 0.53
ABELL0697	0.2820	$9.74^{+2.90}_{-2.13}$	$1.75^{+1.00}_{-0.75}$	$10.2^{+0.8}_{-0.7}$	–	14.58 ± 1.44
ABELL0750	0.1630	$6.30^{+2.71}_{-1.74}$	$3.79^{+2.72}_{-1.68}$	–	–	6.04 ± 0.38
ABELL0773	0.2170	$9.56^{+1.28}_{-1.14}$	$5.67^{+1.58}_{-1.27}$	7.4 ± 0.4	8.64 ± 2.05	8.97 ± 0.52
ABELL0781	0.2984	$6.57^{+1.97}_{-1.65}$	$2.32^{+2.16}_{-1.32}$	$5.5^{+0.7}_{-0.5}$	5.64 ± 2.22	–
ABELL0907	0.1669	$14.28^{+4.59}_{-2.99}$	$1.86^{+0.94}_{-0.72}$	5.4 ± 0.2	6.23 ± 0.45	7.17 ± 0.26
ABELL0963	0.2050	$7.13^{+1.38}_{-1.20}$	$3.77^{+1.38}_{-1.05}$	–	–	7.60 ± 0.37
ABELL1423	0.2130	$4.30^{+1.19}_{-0.97}$	$5.03^{+4.17}_{-2.30}$	–	–	7.04 ± 0.45
ABELL1682	0.2260	$8.66^{+1.38}_{-1.21}$	$3.93^{+1.00}_{-0.83}$	$5.8^{+2.0}_{-1.2}$	–	7.67 ± 0.74
ABELL1689	0.1832	$10.98^{+1.66}_{-1.46}$	$10.56^{+4.31}_{-2.81}$	$8.4^{+0.4}_{-0.3}$	11.23 ± 1.06	10.92 ± 0.32
ABELL1763	0.2279	$16.92^{+3.42}_{-2.70}$	$3.11^{+1.09}_{-0.86}$	8.1 ± 0.5	7.98 ± 1.45	9.09 ± 0.67
ABELL1835	0.2528	$10.09^{+1.88}_{-1.63}$	$6.94^{+4.29}_{-2.35}$	–	11.06 ± 1.09	12.15 ± 0.45
ABELL1914	0.1712	$8.73^{+1.92}_{-1.59}$	$2.64^{+1.03}_{-0.81}$	$8.5^{+0.6}_{-0.4}$	8.57 ± 1.57	9.67 ± 0.50
ABELL2009	0.1530	$7.78^{+3.19}_{-2.03}$	$1.96^{+1.61}_{-0.96}$	–	–	7.37 ± 0.47
ABELL2111	0.2290	$4.93^{+2.68}_{-1.48}$	$4.98^{+9.01}_{-3.92}$	$6.4^{+0.7}_{-0.6}$	–	9.07 ± 0.70
ABELL2204	0.1524	$9.56^{+2.29}_{-1.83}$	$5.17^{+2.10}_{-1.48}$	$8.4^{+0.8}_{-0.6}$	10.50 ± 1.11	14.98 ± 0.72
ABELL2219	0.2281	$10.40^{+2.15}_{-1.75}$	$2.04^{+0.99}_{-0.75}$	–	–	12.80 ± 0.36
ABELL2261	0.2240	$11.93^{+2.18}_{-1.80}$	$2.69^{+0.93}_{-0.74}$	7.3 ± 0.4	–	8.75 ± 0.49
ABELL2390	0.2329	$10.60^{+1.91}_{-1.67}$	$4.11^{+1.15}_{-0.96}$	–	–	15.47 ± 0.68
ABELL2485	0.2472	$5.72^{+1.33}_{-1.13}$	$3.44^{+2.11}_{-1.34}$	–	–	7.37 ± 0.94
ABELL2537	0.2966	$7.65^{+2.31}_{-1.90}$	$8.76^{+10.55}_{-4.29}$	–	8.68 ± 3.78	9.22 ± 0.61
ABELL2552	0.2998	$7.61^{+2.88}_{-2.08}$	$3.20^{+3.16}_{-1.76}$	–	–	10.43 ± 1.34
ABELL2631	0.2779	$7.13^{+2.07}_{-1.66}$	$1.73^{+2.10}_{-1.03}$	$6.9^{+0.8}_{-0.5}$	6.50 ± 1.20	–
ABELL2645	0.2510	$4.16^{+1.15}_{-0.99}$	$3.58^{+2.30}_{-1.39}$	–	–	7.30 ± 1.53
ABELL2813	0.2924	$8.17^{+1.91}_{-1.61}$	$4.99^{+2.96}_{-1.83}$	–	5.48 ± 1.13	–
RXJ1504.1–0248	0.2153	$5.53^{+1.46}_{-1.25}$	$14.75^{+11.69}_{-5.44}$	$9.4^{+1.1}_{-1.0}$	–	15.31 ± 1.09
RXJ1720.1+2638	0.1640	$5.23^{+1.96}_{-1.45}$	$3.27^{+1.96}_{-1.31}$	$6.8^{+0.5}_{-0.3}$	7.46 ± 1.03	9.45 ± 0.48
RXJ2129.6+0005	0.2350	$4.69^{+1.63}_{-1.29}$	$1.44^{+1.51}_{-0.86}$	6.2 ± 0.6	7.62 ± 1.35	8.31 ± 0.44
ZwCl1021.0+0426	0.2906	$5.24^{+1.09}_{-0.96}$	$4.60^{+2.32}_{-1.52}$	–	10.48 ± 2.10	–
ZwCl1459.4+4240	0.2897	$8.54^{+1.22}_{-1.08}$	$3.91^{+0.92}_{-0.77}$	–	6.41 ± 2.76	–

parametrizations obtained are verified to match the three conditions remarkably well in all cases. We list all the fitted parameters (μ, σ) in table 2. Since the logarithm of these distributions follow Gaussian distributions with the usual parameters (μ, σ), we proceed to use linear error propagation for the left-hand side of Eq. (4) with the asymmetrical measurements $\bar{x}_{-\sigma}^{+\sigma}$ symmetrized to $\bar{x}' \pm \Delta x' = \exp(\mu \pm \sigma)$ for the quantities M_{200} , c_{200} and $k_{\text{B}}T_{\text{X}}$. Whenever possible, the error is propagated on the combined logarithmic quantities first, to minimize introduction of bias. We compute the observed virial ratios following Eq. (8) and present them in Fig. 1.

The differences in observed virial ratios reflect the different temperature measurements listed in Table 1 and also plotted in Fig. 2. In view of conflicting data, we build “gold” samples of clusters that have at least two temperature measurements within 1σ of each other, and consider their average (or the average of their logarithms) for the calculations. By inspecting Fig. 2, we selected three gold samples composed of six clusters from M12+M14: ABELL0115, ABELL0209, ABELL0781, ABELL1763, ABELL1914, ABELL2631; one cluster from M12+M16: ABELL0586; and four clusters form M14+M16:

Table 2. Lognormal parameters (μ, σ) for measurements of masses (in units of $h^{-1}10^{14}M_{\odot}$), concentrations and temperatures (from [Maughan et al. 2012](#), in keV) with asymmetrical uncertainties.

Cluster	M_{200}	c_{200}	$k_B T_X$
ABELL0068	(1.93, 0.19)	(1.67, 0.30)	(2.06, 0.13)
ABELL0115	(2.04, 0.31)	(0.68, 0.52)	(1.90, 0.04)
ABELL0209	(2.57, 0.16)	(1.34, 0.25)	(2.00, 0.07)
ABELL0267	(1.81, 0.19)	(1.22, 0.28)	(1.50, 0.10)
ABELL0383	(1.70, 0.22)	(1.56, 0.38)	(1.51, 0.07)
ABELL0521	(1.76, 0.20)	(1.37, 0.35)	(1.57, 0.04)
ABELL0586	(1.97, 0.27)	(2.26, 0.59)	(2.03, 0.11)
ABELL0697	(2.34, 0.25)	(0.72, 0.46)	(2.33, 0.07)
ABELL0750	(1.96, 0.32)	(1.56, 0.50)	–
ABELL0773	(2.27, 0.13)	(1.79, 0.24)	(2.00, 0.05)
ABELL0781	(1.94, 0.27)	(1.14, 0.62)	(1.73, 0.11)
ABELL0907	(2.74, 0.25)	(0.75, 0.41)	(1.69, 0.04)
ABELL0963	(1.99, 0.18)	(1.41, 0.30)	–
ABELL1423	(1.51, 0.24)	(1.89, 0.53)	–
ABELL1682	(2.18, 0.15)	(1.41, 0.23)	(1.85, 0.26)
ABELL1689	(2.42, 0.14)	(2.47, 0.31)	(2.14, 0.04)
ABELL1763	(2.86, 0.18)	(1.21, 0.30)	(2.09, 0.06)
ABELL1835	(2.34, 0.17)	(2.14, 0.41)	–
ABELL1914	(2.20, 0.20)	(1.06, 0.33)	(2.15, 0.06)
ABELL2009	(2.17, 0.31)	(0.94, 0.55)	–
ABELL2111	(1.77, 0.37)	(2.19, 0.91)	(1.87, 0.10)
ABELL2204	(2.30, 0.21)	(1.75, 0.32)	(2.14, 0.08)
ABELL2219	(2.38, 0.18)	(0.84, 0.40)	–
ABELL2261	(2.51, 0.16)	(1.07, 0.29)	(1.99, 0.05)
ABELL2390	(2.39, 0.17)	(1.46, 0.25)	–
ABELL2485	(1.78, 0.21)	(1.42, 0.44)	–
ABELL2537	(2.09, 0.26)	(2.60, 0.62)	–
ABELL2552	(2.12, 0.31)	(1.49, 0.62)	–
ABELL2631	(2.02, 0.25)	(0.96, 0.69)	(1.96, 0.09)
ABELL2645	(1.47, 0.25)	(1.48, 0.45)	–
ABELL2813	(2.14, 0.21)	(1.79, 0.42)	–
RXJ1504.1–0248	(1.76, 0.24)	(2.97, 0.47)	(2.25, 0.11)
RXJ1720.1+2638	(1.75, 0.31)	(1.36, 0.45)	(1.93, 0.06)
RXJ2129.6+0005	(1.62, 0.30)	(0.71, 0.67)	(1.83, 0.10)
ZwCl1021.0+0426	(1.69, 0.19)	(1.67, 0.38)	–
ZwCl1459.4+4240	(1.21, 0.29)	(2.81, 0.57)	–

ABELL0773, ABELL1689, ABELL1835 and ABELL2537 from overlapping error bar clusters. A sample with all eleven clusters from these samples (referred to as GOLD) is also considered.

The Hubble function $H(z)$ in the DfE term must be evaluated in the CDE cosmology, thus depending on the parameters ξ , h and $\Omega_{c0}h^2$. In terms of these parameters, $H(z)$ is given by the Friedmann equation (restricting to the case $w_d = -1$) in the form

$$\left[\frac{H(z)}{100} \right]^2 = h^2 + \Omega_{c0}h^2 \frac{a^{-3(1-\xi)} - 1}{1 - \xi}. \quad (25)$$

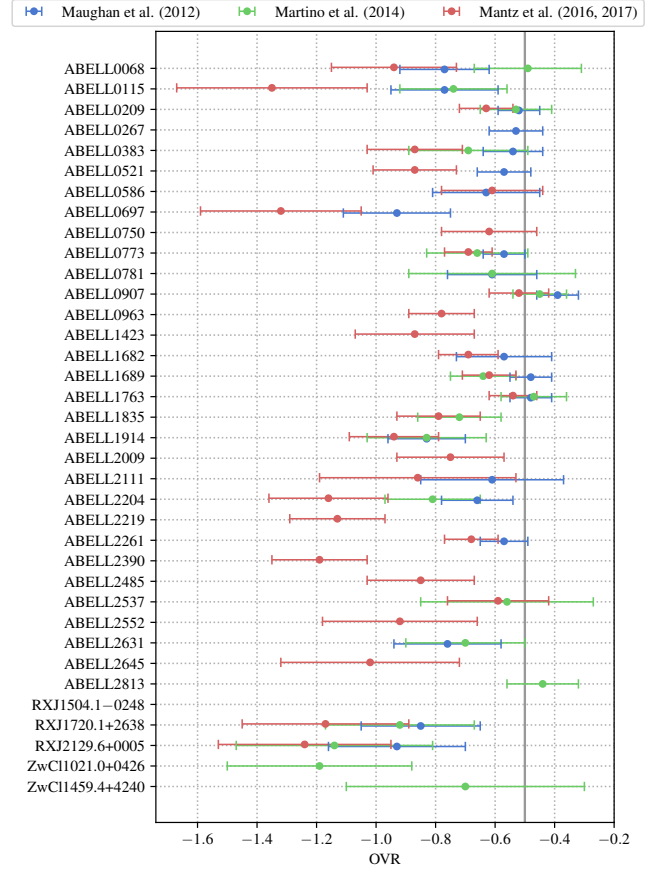


Figure 1. Processed observed virial ratios from the NFW fit parameters data combined X-ray temperatures from different sources. The vertical grey line marks the classic value 0.5.

When w_d is free, $H(z)$ is obtained from the Friedmann equation in its original form with the numerical solutions of Eqs. (1). We then include $H(z)$ from cosmic chronometer data ([Moresco et al. 2016](#)), the JLA supernovae binned dataset ([Betoule et al. 2014](#)) and the local measurement of $H_0 = (73.24 \pm 1.74) \text{ km s}^{-1} \text{ Mpc}^{-1}$ from [Riess et al. \(2016\)](#), joined to the clusters data, in order to perform the analysis outputting h and $\Omega_{c0}h^2$ together with ξ .

3.1 The clusters likelihood

The left-hand side of equation (4), computed from the measurements of mass, temperature and NFW concentration, constitutes our observable, as explained in Sec. 2.2. Denoting by $f_N(x; \mu, \sigma) = (2\pi\sigma^2)^{-1/2} \exp[-(x - \mu)^2 / 2\sigma^2]$ the PDF of a Gaussian distribution $N(\mu, \sigma)$, we assume Gaussian likelihoods $\mathcal{L}_{\text{cluster}} = f_N(\text{EVR} - \text{DfE}; \mu, \sigma)$ for each cluster, with μ and σ given by the nominal value and standard deviation of the quantity $\text{OVR} - \text{DfE}$, to compare the predicted values of the equilibrium virial ratio $\text{EVR}(\xi) \equiv -(1 - 6\xi) / (2 + 3\xi)$ with this observable.

The total likelihood of a set of clusters is given by the product $\mathcal{L}_{\text{clusters}} = \prod_i \mathcal{L}_{\text{cluster } i}$ of the likelihoods of all the clusters in the given sample. We should stress that the left-hand side of equation (4) depends on the amount of matter and the Hubble parameter through Ω_{c0} and H_0 , or equivalently $\Omega_{c0}h^2$ and h , motivating us to include $H(z)$ and supernovae data. The parameters ξ and γ are

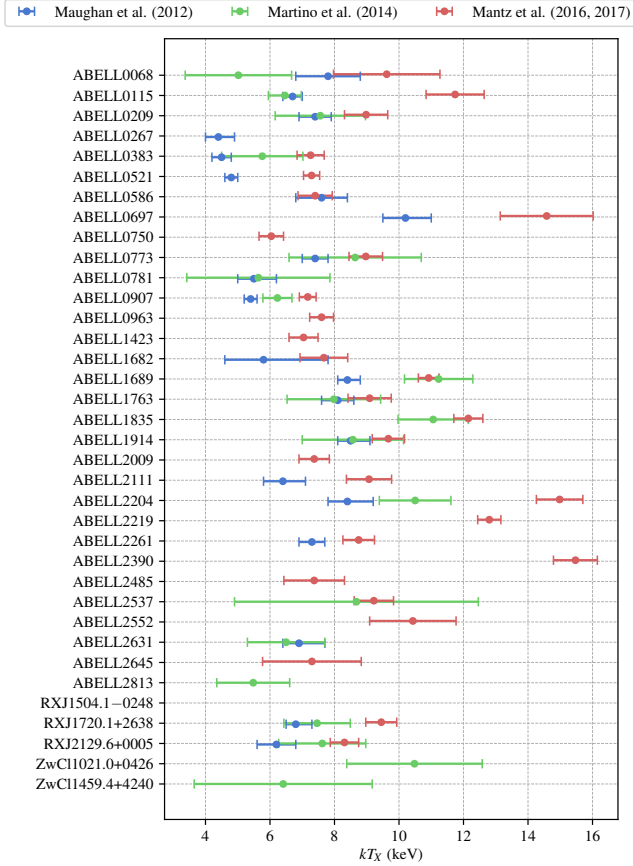


Figure 2. X-ray temperatures from different sources. Values are listed in Table 1.

also implicit in the likelihood $\mathcal{L}_{\text{cluster}}$ through the DFE term. $\mathcal{L}_{\text{clusters}}$ is thus also multiplied by the product of the Gaussian likelihoods $\mathcal{L}_{H(z)} = \prod_i f_N(H(z_i)_{\text{predicted}}; H(z_i), \sigma_{H(z_i)})$ of the $H(z)$ data and by the JLA likelihood \mathcal{L}_{JLA} , based on estimates of binned distance modulus obtained from the JLA supernovae sample (from [Betoule et al. 2014](#)): $\mathcal{L}_{\text{total}} = \mathcal{L}_{\text{clusters}} \times \mathcal{L}_{H(z)} \times \mathcal{L}_{\text{JLA}}$. An additional nuisance parameter ΔM is included to account for a possible shift in the absolute magnitudes of the supernovae.

We thus obtain the unnormalized posterior distribution probabilities $P(\theta | D)$, for our set of parameters $\theta = \{\xi, h, \Omega_{c_0} h^2, \gamma, \Delta M\}$ given the data D by using Bayes' theorem

$$P(\theta | D) = \frac{\mathcal{L}_{\text{total}}(D | \theta) \pi(\theta)}{P(D)}, \quad (26)$$

where $\pi(\theta)$ is the prior probability for the parameters, assumed flat and detailed in section 4. The correct normalization of the posterior distribution is given by the marginal likelihood or evidence $P(D)$, which is not required for our parameter inference purposes.

4 THE MCMC ANALYSES

Using the EPIC code ([Marcondes 2017](#)), we run MCMC simulations for our interacting model with fixed $w_d = -1$ using each of the four samples considered above and with w_d using the GOLD sample. The clusters data are combined with $H(z)$ and supernovae data in all cases. We set flat priors over the intervals $[-0.2, 0.2]$ for

Table 3. Constraints on the interaction strength parameter ξ and the derived parameter $\text{EVR}(\xi)$ of the CDE model from $H(z)$ data, supernovae data and each of the clusters samples M12+M14, M12+M16, M14+M16 and GOLD.

Parameter	Sample	Best-fitting	1 σ C.L.	2 σ C.L.
100 ξ	M12+M14	-1.90	$-1.86^{+1.23}_{-1.28}$	$-1.86^{+2.62}_{-2.47}$
	M12+M16	-2.29	$-1.83^{+4.65}_{-4.43}$	$-1.83^{+10.42}_{-8.45}$
	M14+M16	-3.90	$-3.94^{+1.58}_{-1.44}$	$-3.94^{+3.38}_{-2.81}$
	GOLD	-2.85	$-2.70^{+0.90}_{-0.91}$	$-2.70^{+1.82}_{-1.81}$
	GOLD (w_d free)	-3.05	$-2.79^{+0.94}_{-0.93}$	$-2.79^{+1.97}_{-1.79}$
$\text{EVR}(\xi)$	M12+M14	-0.57	-0.57 ± 0.05	-0.57 ± 0.10
	M12+M16	-0.59	$-0.55^{+0.17}_{-0.19}$	$-0.55^{+0.36}_{-0.37}$
	M14+M16	-0.66	$-0.66^{+0.07}_{-0.06}$	$-0.66^{+0.14}_{-0.12}$
w_d	GOLD	-0.61	$-0.61^{+0.04}_{-0.03}$	$-0.61^{+0.08}_{-0.07}$
	GOLD (w_d free)	-0.62	-0.61 ± 0.04	$-0.61^{+0.08}_{-0.07}$

ξ , [0.5, 0.9] for h , [0.0, 0.3] for $\Omega_{c_0} h^2$, [0.00, 0.99] for γ , [-1.0, 1.0] for ΔM and [-2.0, -0.4] for w_d when it is free. The code evolved 12 independent Markov chains in each case, the convergence, according to the Gelman-Rubin criteria for multivariate distributions ([Gelman & Rubin 1992](#); [Brooks & Gelman 1998](#)), being checked with the multivariate potential scale reduction factor \hat{R}^p for p parameters within about 5×10^{-3} of 1.

The constraints on ξ and EVR and w_d are given in Table 3 at 1 σ and 2 σ confidence levels (C.L.); the other parameters are given in Table A1. In Fig. 3 we plot the marginalized distributions of the parameters ξ , γ and the joint-posterior distribution of ξ and w_d when this is also free, with the sample GOLD. We note that the analysis with w_d free has no effect on the marginalized distribution of the interaction constant (the corresponding violet and brown curves are almost indistinguishable), although it does affect the distribution of $\Omega_{c_0} h^2$ (not plotted).

5 RESULTS

Constraints with sample M12+M16 are compatible with $\xi = 0$ within 1 σ , while M12+M14, M14+M16, GOLD and GOLD with w_d free give 1.44 σ , 2.30 σ , 2.80 σ and 2.77 σ detections, respectively. When we let the dark energy equation-of-state parameter vary, it can be noted from the joint-posterior distribution that w_d and ξ are not correlated, hence the constraints on ξ (and also on all other parameters except $\Omega_{c_0} h^2$) are practically unchanged. This can be seen in the lack of strong difference in Fig. 3 between the two GOLD distributions.

If we disregard the M12+M16 sample, as it only contains one cluster, it appears that we have 2 σ to 3 σ detection of the DE-DM interaction, a slight improvement on previous results of the virial detection idea (e.g. [Bertolami et al. 2007](#)). As discussed previously, the main problem appears from the inconsistent X-ray temperature detections, with no present guiding principle to favour one dataset over another. We turned the difficulty by selecting in the three datasets available to us that contained consistent clusters and compiled them in a GOLD sample. The method clearly improves detection when stacking as many clusters as possible: the distributions for ξ and EVR on Fig. 3 are more peaked for larger samples.

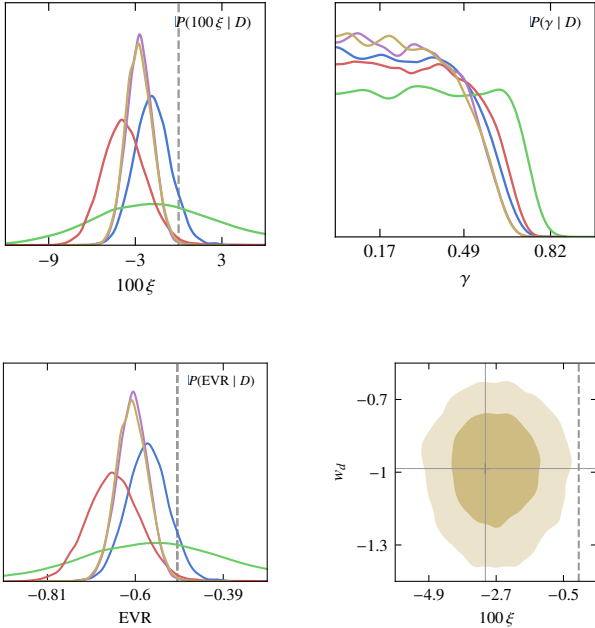


Figure 3. Marginalized distributions of ξ , γ and $\text{EVR}(\xi)$ for the samples M12+M14 (blue), M12+M16 (green), M14+M16 (red), GOLD with w_d fixed (violet) and GOLD with w_d free (brown). Dashed grey lines mark the no-interaction values $\xi = 0$ and $\text{EVR} = -0.5$. The last panel shows the two-dimensional joint-posterior distribution of the parameters ξ and w_d when this parameter is free, using the sample GOLD.

6 DISCUSSION AND CONCLUSIONS

In this paper we have continued the works of Bertolami et al. (2007); Le Delliou et al. (2007); Bertolami et al. (2008, 2009, 2012); Abdalla et al. (2009, 2010); He et al. (2010); Le Delliou et al. (2015) on virial detection of dark sector interaction. The approach of Le Delliou et al. (2015) for non-virialised clusters was improved to obtain consistent results. Based on evaluation of the dynamical out-of-equilibrium state independent of the details of each cluster’s astrophysical history, the method relies on a set of simplifying reasonable assumptions. Although the convergence ansatz could be debatable, its general features prove to provide enough power to the method so as to be able to yield consistent results. From a sample of 50 clusters with full necessary data, consistency led us to trim down to a maximum of 11 clusters. The results range from no detection, but for a single cluster sample, to 3σ detection, with improvement when the samples are larger. This is a strong indication that the method is sound and likely to yield a clear answer to dark sector interaction question, given larger samples of clusters, with clear guidance on the X-ray temperature detection reliability and robust weak lensing determination.

This is why the detection of interaction in the dark sector (or its ruling out) will greatly benefit from future instruments and surveys. In particular, increasing the number of clusters with mass distribution measurements through lensing effects (which need deep imaging and large field-of-view) with the next generation of telescopes, such as the Thirty Meter Telescope (TMT, Skidmore & TMT International Science Development Teams & TMT Science Advisory Committee 2015), the Giant Magellan Telescope (GMT, Johns et al. 2012) and the European Extremely Large Telescope (E-ELT, McPherson et al. 2012). Likewise, the X-ray detected clusters

will increase in the next few years with the extended ROentgen Survey with an Imaging Telescope Array (*eROSITA*, Merloni et al. 2012). With these perspectives in observations and the method finalised here, we are confident that a reliable dark sector interaction detection is within reach.

7 ACKNOWLEDGEMENTS

We thank Nobushiro Okabe for generously sharing with us his NFW fits of the LoCuSS clusters. The work of M.Le D. has been supported by Lanzhou University starting fund and PNPd/CAPES20132029. M.Le D. also wishes to acknowledge DFMA/IF/USP and IFT/UNESP where this work was initiated. G.B.L.N. thanks financial support from CNPq and FAPESP (2018/17543-0).

REFERENCES

- Abdalla E., Abramo L. R., Sodré L., Wang B., 2009, *Phys. Lett. B*, 673, 107
 Abdalla E., Abramo L. R., de Souza J. C. C., 2010, *Phys. Rev. D*, 82, 023508
 Ade P. a. R., et al., 2014, *A&A*, 571, A16
 Amendola L., 2000a, *Phys. Rev. D*, 62, 043511
 Amendola L., 2000b, *MNRAS*, 312, 521
 Bertolami O., Gil Pedro F., Le Delliou M., 2007, *Phys. Lett. B*, 654, 165
 Bertolami O., Gil Pedro F., Le Delliou M., 2008, *EAS Publ. Ser.*, 30, 161
 Bertolami O., Gil Pedro F., Le Delliou M., 2009, *Gen. Relativ. Gravit.*, 41, 2839
 Bertolami O., Gil Pedro F., Le Delliou M., 2012, *Gen. Relativ. Gravit.*, 44, 1073
 Betoule M., et al., 2014, *A&A*, 568, A22
 Brooks S. P., Gelman A., 1998, *J. Comput. Gr. Stat.*, 7, 434
 Cao S., Liang N., 2013, *Int. J. Mod. Phys. D*, 22, 1350082
 Clowe D., Bradač M., Gonzalez A. H., Markevitch M., Randall S. W., Jones C., Zaritsky D., 2006, *ApJ*, 648, L109
 Costa A. A., Xu X.-D., Wang B., Abdalla E., 2017, *J. Cosmol. Astropart. Phys.*, 1701, 028
 Del Popolo A., Gambera M., Recami E., Spedicato E., 2000, *A&A*, 353, 427
 Gelman A., Rubin D. B., 1992, *Stat. Sci.*, 7, 457
 He J.-H., Wang B., Abdalla E., Pavon D., 2010, *J. Cosmol. Astropart. Phys.*, 1012, 022
 Henriksen R. N., Widrow L. M., 1995, *MNRAS*, 276, 679
 Henriksen R. N., Widrow L. M., 1997, *Phys. Rev. Lett.*, 78, 3426
 Henriksen R. N., Widrow L. M., 1999, *MNRAS*, 302, 321
 Jee M. J., Hughes J. P., Menanteau F., Sifón C., Mandelbaum R., Barrientos L. F., Infante L., Ng K. Y., 2014, *ApJ*, 785, 20
 Johns M., et al., 2012, in Proc. SPIE. International Society for Optics and Photonics, p. 84441H, doi:10.1117/12.926716
 Le Delliou M., 2008, *A&A*, 490, L43
 Le Delliou M., Henriksen R. N., 2003, *A&A*, 408, 27
 Le Delliou M., Bertolami O., Gil Pedro F., 2007, *AIP Conf. Proc.*, 957, 421
 Le Delliou M., Marcondes R. J. F., Lima Neto G. B., Abdalla E., 2015, *MNRAS*, 453, 2
 MacMillan J. D., Widrow L. M., Henriksen R. N., 2006, *ApJ*, 653, 43
 Mantz A. B., et al., 2016, *MNRAS*, 463, 3582
 Mantz A. B., et al., 2017, *MNRAS*, 467, 3443
 Marcondes R. J. F., 2017, preprint (arXiv:1712.00263 [astro-ph.IM])
 Martino R., Mazzotta P., Bourdin H., Smith G. P., Bartalucci I., Marrone D. P., Finoguenov A., Okabe N., 2014, *MNRAS*, 443, 2342
 Maughan B. J., Giles P. A., Randall S. W., Jones C., Forman W. R., 2012, *MNRAS*, 421, 1583
 McPherson A., Spyromilio J., Kissler-Patig M., Ramsay S., Brunetto E., Dierickx P., Cassali M., 2012, in Proc. SPIE. International Society for Optics and Photonics, p. 84441F, doi:10.1117/12.927787
 Merloni A., et al., 2012, preprint (arXiv:1209.3114 [astro-ph.HE])

Monteiro-Oliveira R., Cypriano E. S., Machado R. E. G., Lima Neto G. B., Ribeiro A. L. B., Sodr e L., Dupke R., 2017, *MNRAS*, 466, 2614
Moresco M., et al., 2016, *J. Cosmol. Astropart. Phys.*, 1605, 014
Navarro J. F., Frenk C. S., White S. D. M., 1996, *ApJ*, 462, 563
Okabe N., Smith G. P., 2016, *MNRAS*, 461, 3794
Perlmutter S., et al., 1999, *ApJ*, 517, 565
Riess A. G., et al., 1998, *AJ*, 116, 1009
Riess A. G., et al., 2016, *ApJ*, 826, 56
Skidmore W., TMT International Science Development Teams & TMT Science Advisory Committee 2015, *Res. Astron. Astrophys.*, 15, 1945
Zwicky F., 1933, *Helv. Phys. Acta*, 6, 110
Zwicky F., 1937, *ApJ*, 86, 217

APPENDIX A: CONSTRAINTS ON THE OTHER PARAMETERS

Completing Table 3, we present here in Table A1 the remaining constraints on the other parameters of our analyses. The confidence intervals reported for γ without central values reflect the fact that its distributions are poorly constrained, only suppressed by the singularity as γ approaches 1 but otherwise flat. The exact values at which the distributions become suppressed are sensitive to our arbitrary choice of $t_0 = 1 \text{ km}^{-1} \text{ s Mpc}$ (see Sec. 2.2.2). However, this does not affect our results, which are based on marginalizing this parameter over all values allowed by our priors. Constraints on the parameters Ω_{c0} and Ω_{d0} derived from $\Omega_{c0}h^2$ and h are also listed.

This paper has been typeset from a \LaTeX file prepared by the author.

Table A1. Constraints on parameters of CDE model from $H(z)$ data, supernovae data and each of the clusters samples M12+M14, M12+M16, M14+M16 and GOLD.

Parameter	Group	Best-fitting	1σ C.L.	2σ C.L.
h	M12+M14	0.72	$0.72^{+0.01}_{-0.02}$	$0.72^{+0.02}_{-0.03}$
	M12+M16	0.72	$0.71^{+0.02}_{-0.01}$	$0.71^{+0.03}_{-0.02}$
	M14+M16	0.71	$0.72^{+0.01}_{-0.02}$	$0.72^{+0.02}_{-0.03}$
	GOLD	0.71	$0.71^{+0.02}_{-0.01}$	$0.71^{+0.03}_{-0.02}$
	GOLD (w_d free)	0.71	$0.71^{+0.02}_{-0.01}$	$0.71^{+0.03}_{-0.02}$
$\Omega_{c0}h^2$	M12+M14	0.13	$0.13^{+0.02}_{-0.01}$	$0.13^{+0.03}_{-0.02}$
	M12+M16	0.13	$0.13^{+0.03}_{-0.02}$	$0.13^{+0.06}_{-0.03}$
	M14+M16	0.13	0.13 ± 0.01	0.13 ± 0.02
	GOLD	0.13	0.13 ± 0.01	0.13 ± 0.02
	GOLD (w_d free)	0.14	$0.15^{+0.02}_{-0.03}$	$0.15^{+0.04}_{-0.07}$
γ	M12+M14	0.03	$0 < \gamma \leq 0.41$	$0 < \gamma \leq 0.61$
	M12+M16	0.20	$0 < \gamma \leq 0.64$	$0 < \gamma \leq 0.71$
	M14+M16	0.10	$0 < \gamma \leq 0.43$	$0 < \gamma \leq 0.63$
	GOLD	0.01	$0 < \gamma \leq 0.39$	$0 < \gamma \leq 0.57$
	GOLD (w_d free)	0.11	$0 < \gamma \leq 0.38$	$0 < \gamma \leq 0.57$
ΔM	M12+M14	0.04	0.04 ± 0.04	$0.04^{+0.08}_{-0.09}$
	M12+M16	0.04	0.04 ± 0.04	$0.04^{+0.08}_{-0.09}$
	M14+M16	0.03	$0.03^{+0.05}_{-0.04}$	$0.03^{+0.09}_{-0.08}$
	GOLD	0.03	0.04 ± 0.04	$0.04^{+0.08}_{-0.09}$
	GOLD (w_d free)	0.04	0.04 ± 0.04	0.04 ± 0.09
Ω_{c0}	M12+M14	0.26	$0.26^{+0.03}_{-0.02}$	$0.26^{+0.06}_{-0.05}$
	M12+M16	0.26	$0.26^{+0.05}_{-0.04}$	$0.26^{+0.12}_{-0.07}$
	M14+M16	0.25	$0.25^{+0.02}_{-0.03}$	0.25 ± 0.05
	GOLD	0.25	$0.26^{+0.02}_{-0.03}$	$0.26^{+0.04}_{-0.05}$
	GOLD (w_d free)	0.28	$0.29^{+0.04}_{-0.06}$	$0.29^{+0.09}_{-0.13}$
Ω_{d0}	M12+M14	0.74	$0.74^{+0.02}_{-0.03}$	$0.74^{+0.05}_{-0.06}$
	M12+M16	0.74	$0.74^{+0.04}_{-0.05}$	$0.74^{+0.07}_{-0.12}$
	M14+M16	0.75	$0.75^{+0.03}_{-0.02}$	0.75 ± 0.05
	GOLD	0.75	$0.74^{+0.03}_{-0.02}$	$0.74^{+0.05}_{-0.04}$
	GOLD (w_d free)	0.72	$0.71^{+0.06}_{-0.04}$	$0.71^{+0.13}_{-0.09}$